Improved switching characteristics of TiO_{2-x} ReRAM with embedded ultra-thin Al_2O_{3-y} layers

Maria Trapatseli, Simone Cortese, Alexantrou Serb, and Themistoklis Prodromakis*
Nano Group, School of Electronics and Computer Science,
University of Southampton, Southampton SO17 1BJ, U.K.
(Dated: March 7, 2017)

Transition metal-oxide resistive random access memory (RRAM) devices have demonstrated excellent performance in switching speed, versatility of switching and low-power operation. However, this technology still faces challenges like poor cycling endurance, degradation due to high electroforming switching voltages and low yields. Engineering of the active layer by doping or addition of thin oxide buffer layers, are approaches that have been often adopted to tackle these problems. Here, we have followed a strategy that combines the two; we have used ultra-thin Al_2O_{3-y} buffer layers incorporated between TiO_{2-x} thin films taking into account both 3+/4+ oxidation states of Al/Ti cations. Our devices were tested by DC and pulsed voltage sweeping and in both cases demonstrated improved switching voltages. We believe that the Al_2O_{3-y} layers act as reservoirs of oxygen vacancies which are injected during EF, facilitate a filamentary switching mechanism and provide enhanced filament stability as shown by the cycling endurance measurements.

I. INTRODUCTION

Resistive Random Access Memory (RRAM) devices have been in the spotlight for over 30 years, for their potential as next-generation non-volatile memories. Their simple metal-insulator-metal (MIM) structure as well as their high speed operation, high density and low-power consumption [1], makes them strong competitors to Flash and DRAM. Their potential is not limited in their promising performance but it extends to intricate tailorability of materials and sophisticated architectures, that could lead in ultra-high density 3D integrated structures. These devices, usually need a dielectric soft-breakdown (SB) supplied by an electroforming (EF) step before they can start toggling between a low resistive state (LRS) and a high resistive state (HRS). The EF step is often realised as the creation of a conductive path inside the oxide matrix, which facilitates the resistive switching (RS). Depending on the combination of oxide active layer and metal electrodes used, the contributions of different carriers to the RS mechanism may vary. In transition metal oxide systems, oxygen vacancies and metal cation interstitials are believed to play [1] the key role. Due to this ionic nature of RS, some oxides like TiO_{2-x} can support different modes of RS, such as analog and binary switching [2]. Another interesting property of RRAM devices is volatility (short-term resistance drift towards higher values), which doesn't favour memory applications but it is very interesting for applications such as real-time neuronal signal detection [3].

Although RRAM devices have demonstrated fascinating characteristics, they still suffer poor cycling endurance, device degradation due to high switching/EF voltages and low yields. Among the different approaches adopted to tackle these challenges, doping of the active layer [4, 5] and addition of complementary oxide thin films [6–8] were the most common. In TiO_2, dopants with a suitable oxidation state could successfully reduce the energy required for EF and the conducting filament variability, according to a theoretical study by Zhao *et al.* [4]. In a previous work, we demonstrated the reduction of switching and EF voltages in TiO_{2-x} RRAM devices by Al doping, due to possible reduction of oxygen vacancy formation energy triggered by the 4+ and 3+ oxidation states of Ti and Al.

In another study by Goux *et al.*, Al_2O_3 thin films were used in combination with the main active layer (HfO_2) for lower operation currents and switching voltage tuning [6]. Wang *et al.* used trilayer $Al_2O_3/HfO_2/Al_2O_3$ structures in RRAM devices, to improve the resistive switching characteristics by filament formation/rupture at the Al_2O_3/HfO_2 interfaces [9]. Wu *et al.* deposited a AlO_δ barrier layer on Ta_2O_{5-x}/TaO_y bilayers and achieved improved resistive switching performance with $>10\ \mu A$ switching current, $> 10^{11}$ cycling endurance and stable multilevel states [10].

In the present work we present a different approach to improve RRAM switching parameters, by incorporating thin Al_2O_{3-y} layers within the TiO_{2-x} active layer. A systematic study was carried out showing the best performance was achieved with 2 Al_2O_{3-y} layers.

Figure 1. (a)Conceptual sketch of the filament formation in a TiO_{2-x}-based ReRAM device and (b) in a TiO_{2-x}-Al_2O_{3-y}-TiO_{2-x}-based device, depicting a stable filament segment formed in the Al_2O_{3-y} layer. (c) Portrays the four different ReRAM active layer configurations that were developed for this work.

* Corresponding author: Maria Trapatseli, mt3c13@soton.ac.uk
Group's website: www.nanomemristors.com

Figure 2. (a) XPS survey sprectra from single $TiO_{2\text{-}x}$ and $Al_2O_{3\text{-}y}$ thin films deposited on Si substrates, (b), (c) and (d) Al 2*p* XPS depth profile core level spectra from T1, T2 and T3 multilayer stacks, accordingly.

II. EXPERIMENTAL METHODS

A. Thin Film Fabrication and Characterisation

Table I. Nominal thickness of the oxide thin films that compose the multilayer stacks.

	T0	**T1**	**T2**	**T3**
$TiO_{2\text{-}x}$	46 nm	23 nm	23 nm	11 nm
$Al_2O_{3\text{-}y}$		2 nm	2 nm	2 nm
$TiO_{2\text{-}x}$		23 nm	11 nm	11 nm
$Al_2O_{3\text{-}y}$			2 nm	2 nm
$TiO_{2\text{-}x}$			23 nm	11nm
$Al_2O_{3\text{-}y}$				2 nm
$TiO_{2\text{-}x}$				11 nm

$TiO_{2\text{-}x}$ and $Al_2O_{3\text{-}y}$ multilayer stacks were deposited by reactive sputtering (Helios XL, Leybold Optics) from Ti and Al metal targets (99.99% purity), on p-type Si chips cleaned in methanol and isopropanol. The settings during the $TiO_{2\text{-}x}$ thin film deposition were 8 sccm O_2 and 35 sccm Ar at the Ti cathode, operating at 2 kW. The $Al_2O_{3\text{-}y}$ thin films were deposited at 100 W power, with 15 sccm O_2 at the Al cathode and 25 sccm Ar at the plasma beam source. The thin films were deposited subsequently one after the other, without breaking the vacuum, to ensure better adhesion and better quality of the interfaces. The thickness of the $TiO_{2\text{-}x}$ thin films was 11 and 23 nm and the thickness of the $Al_2O_{3\text{-}y}$ thin films was approximately 2 nm, but the total thickness of each thin film stack was maintained 44-46 nm for fair comparison between ReRAM devices comprising this thin film stacks as active layers. Figure 1 (c) depicts the 4 different stack configurations comprising the $TiO_{2\text{-}x}$ and $Al_2O_{3\text{-}y}$ thin films. Table I is listing the nominal thickness of the thin films used to compose the multilayer stacks. The thickness of each layer was evaluated by Spectroscopic Ellipsometry (Woollam M-2000) using the Cody-Lorentz model and the total thickness of each stack by Contact Profilometry (KLA-Tencor P11).

Thin film elemental characterisation was carried out using a Thermo Scientific Theta Probe Angle-Resolved X-ray Photoelectron Spectrometer with an Al Kα X-ray source (hv=1486.6 eV), operating at 2×10^{-9} mbar. The X-ray source operated at 6.7 mA emission current and 15 kV anode bias. Core level and survey spectra were collected over an area of 400×400 μm^2 with pass energy of 200 and 50 eV, respectively. XPS depth profile measurements were carried out using an argon ion gun operating at 1kV/1μA, etching an area of 2×2 mm^2 with each etching step lasting 40 s. Photoelectrons were collected at a base pressure of 5×10^{-7} mbar after every etching phase, from the exposed by the ion gun surface, until the whole stack was etched through and Si was the only detectable element. C 1*s* core level due to adventitious carbon, was always present in the spectra and was used for charge shift correction. All spectra were collected and analysed with the Avantage data system. ReRAM devices were fabricated on Si/SiO_2(200 nm)/Ti(5 nm) supports. The electrodes and active layer were patterned by Optical Lithography. 10 nm Pt bottom and top electrodes were evaporated in an Electron-beam Evaporator followed by lift-off. The active layer was deposited by reactive sputtering as described in detail above.

B. ReRAM Device Fabrication and Testing

Finished 40×40 μm^2 standalone ReRAM devices were electrically characterised with a Keithley SCS-4200 Semiconductor Device Analyser. During the electroforming (EF) and DC I-V sweeps, the bias was applied on the top electrode, while the bottom electrode was connected to the ground. The devices were also characterised with pulsed voltage sweeping using ArC ONE^{TM}, a custom-made PCB-based system for device testing and characterisation [11]. The devices were electroformed and tested for switching using the algorithms presented in [12] and [13] accordingly, as well as for endurance.

III. RESULTS

A. Thin Film Characterisation

Figure 2 (a) displays the XPS survey spectra recorded from two reference $TiO_{2\text{-}x}$ and $Al_2O_{3\text{-}y}$ thin films deposited on Si, 23 nm and 2 nm thick, respectively. The $TiO_{2\text{-}x}$ thin film survey (red), displays the following peaks from photoemission: O 2*s*, Ti 3*p*, Ti 3*s*, C 1*s*, Ti 2*p* and Ti 2*s*. The Ti 2*p* peak is a doublet, and can be ascribed to 4+ oxidation state, indicating that the $TiO_{2\text{-}x}$ thin film is near-stoichiometric. The $Al_2O_{3\text{-}y}$ thin film survey (black) exhibited the following peaks from photoemission: O 2*s*, Al 2*p*, Si 2*p*, Al 2*s*, Si 2*s*, C 1*s*, and O 1*s*. Due to the high surface sensitivity of XPS, Si 2*s* and Si 2*p* peaks were detected in the survey spectrum and are associated to Si phototoelectrons from the Si substrate. As XPS photoelectrons can be extracted only from the top ∼5 nm of the sample, the presence of the Si peaks is another proof of the $Al_2O_{3\text{-}y}$ thin film thickness. Due to the very low intensity of the peaks ascribed to Al, the stoichiometry of the $Al_2O_{3\text{-}y}$ thin film was not assessed at this point. Figures 2(b), (c) and (d) portray the Al 2*p*

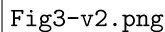

Figure 3. (a) Box plot of electroforming voltages, (b) mean SET and RESET voltage scatter plots (whiskers are indicating the standard deviation) concerning the number of Al_2O_{3-y} layers in each device configuration. (c), (d), (e) and (f) display I-V charactersitics obtained from the device stacks T0, T1, t2 and T3, respectively. Insets portray the typical electroforming step of each device configuration.

150 core level depth profiling spectra that were recorded from 151 the samples T1, T2 and T3 accordingly. Grey-shaded 152 squares are indicating the positions of the Al 2p peaks in 153 each set of selected XPS spectra. The minimum allowed 154 ion gun energy of 1kV/1μA and small etching step of 40 s 155 were used to ensure that the intermediate Al_2O_{3-y} layers 156 will not be etched through. Although the Al_2O_{3-y} lay157 ers are ultra-thin and despite the inter-diffusion between 158 the subsequently deposited layers during sputtering, Al 159 2p core level is still detectable, confirming that the stack 160 configuration is maintained. It is possible that a mixed 161 phase of the two oxides could be formed at each interface, 162 but due to the low deposition temperature we believe that 163 a compound comprising both Al and Ti is unlikely. How-

ever, this argument cannot be currently confirmed with this technique. Another observation from the XPS depth profiling spectra was that Ti $2p$ intensity was minimum when the Al $2p$ was maximum. Similarly, the Al $2p$ peak was completely disappearing when etching in the $TiO_{2\text{-}x}$.

B. Devices Characterisation

1. DC voltage sweeping

The finished 40×40 μm^2 standalone ReRAM devices comprising the active layers T0-T4, were tested with DC voltage sweeping to assess their switching characteristics. The resistance of the pristine devices was in the range of GOhms and they needed an electroforming step to start switching repeatably between two resistive states. Figure 3 (a) portrays the box plots (n=10) of the devices with respect the number of $Al_2O_{3\text{-}y}$ layers they comprise. The upper and lower horizontal lines of each box resemble the 25% and 75% percentiles, respectively, while the inner horizontal line the median. The mean EF voltage increases slightly from -5.0 V to -5.2 V, -5.4 V and -5.3 V for the the devices comprising 1, 2 and 3 $Al_2O_{3\text{-}y}$ layers, respectively, probably due to the very good insulating properties of $Al_2O_{3\text{-}y}$. However, EF voltage distribution is decreased in all devices that contain $Al_2O_{3\text{-}y}$ layers, indicating that the addition of $Al_2O_{3\text{-}y}$ layers can reduce the variability of EF voltages.

Figure 3 (b) displays the mean SET and RESET voltage plots from devices (n=5) that switched repetitively, with the whiskers indicating the standard deviation. The mean SET voltage dropped from 2.53 V for the T0 devices to 2.30 V, 2.18 V and 2.29 V for the devices T1, T2 and T3, accordingly. The SET standard deviation decreased for the T1 and T2 devices but deteriorated for the T3 devices. Similarly, the mean RESET voltage decreased from -2.00 V for the T0 devices to -1.53 V, -1.74 V and -1.66 V for the T1, T2 and T3, respectively. The RESET voltage standard deviation, follows a similar trend with the SET equivalent and decreases for devices T1, T2 and T3 but not with a clear trend. Among all configurations comprising $Al_2O_{3\text{-}y}$ layers, T3 is possibly the one with the worst SET/RESET performance. Figures 3 (c), (d), (e) and (f) portray DC I-V characteristics from T0, T1, T2 and T3 devices after EF. Each panel displays three I-V characteristics, all from well behaved devices that switched repetitively. It can be observed, that devices of the same configuration had very similar switching behaviour, but this behaviour was found to vary among different configurations.

A typical EF step for every device configuration is displayed as inset in Figures 3 (c), (d), (e) and (f) and it is not revealing any particular difference associated with the number of $Al_2O_{3\text{-}y}$ layers in the devices. Following the EF which was performed in negative polarity (and altered the device resistance from the pristine state to HRS), the voltage was swept from 0 to 3 V and back to 0 with 10^{-4} A current compliance, switching the devices from HRS to LRS. The devices' resistance switched back to HRS when the voltage was swept from 0 to -3 V and back to 0 with 10^{-3} A current compliance. SET was observed during a positive voltage sweep and RESET during a negative voltage sweep. Both the I-V characteristics exhibited an exponential dependence between voltage and current. This dependence suggests that the filament does not have metallic properties. SET usually emerged as an abrupt transition (with an exception in the case of T2 as shown in Figure 3 (e)), therefore, lower current compliance was used to protect the device from an unwanted hard-breakdown (HB). During an undesirable HB, the current dependence in LRS is linear, possibly suggesting a fully connected filament to the electrode, however, that was not observed in these devices due to current compliance. Overall, devices T1 and T2 show improved SET and RESET voltages, small variability of I-V characteristics among different devices, at the expense of slightly higher EF voltage compared to T0 (4% and 8% for T1 and T2. respectively).

2. Pulse voltage sweeping

Testing ReRAM devices with DC voltage sweeping gives a lot of information about the mechanism but is also known to induce device degradation [14, 15]. Therefore, we also performed pulse voltage sweeping to our devices to evaluate their resistive switching performance in this operation condition. The device EF was carried out using the same algorithm presented in [16], performed in three voltage ramp stages (positive-negative-positive), each stage having a considerable effect on the device's resistance. Figure 4 (a) displays an example of a complete EF. The 3-stage EF was necessary to drop the device's resistance below 50 kOhm, which was a non-volatile regime where devices behaved more reliably. Different ramp polarity combinations were attempted, however, the above mentioned combination was chosen for achieving the highest EF yield.

Table II. The settings used during electroforming and pulse voltage sweeping of the T0-T3 devices.

Parameter	Electro-forming	Switching
Start write pulse amplitude (V)	0.2	0.2
Write pulse amplitude step (V)	0.2	0.1
End write pulse amplitude (V)	11	4
Write pulse width (ms)	0.1	0.1
Read pulse amplitude (V)	0.2	0.2
No. of write pulses	10	10
No. of read pulses	5	5
Series resistance (kOhm)	100	-
Resistance threshold (kOhm)	50	-

Following the EF, the devices were switched implementing the algorithm presented in [13]. The algorithm applies ramps of increasing in amplitude voltage pulses, assess the device's resistance between each pulse streak and between ramps and reverses the ramp when a resis-

tance threshold is exited. The settings for the switching are depicted in Table II. Devices from all categories, operated in different resistance ranges, but the most well-behaved ones (more repeatable, without resistance drift) usually operated in the range of 5-60 kOhm. Figure 4 (b) displays the mean switching voltages calculated from 5 devices from each stack category with whiskers representing the standard deviation of the switching voltages. It can be observed that the mean switching voltage and standard deviation decrease considerably for the devices T2 and T3. Figure 5 (a), (b), (c) and (d) display the resistive states of typical T0, T1, T2 and T3 devices, respectively, that operated within the range 5-20 kOhm.

The devices were tested for cycling endurance using the ArC ONE system. Programming pulses of fixed amplitude and width were applied in alternating polarities and the resistive state was assessed after each pulse at a read voltage of 0.2 V. As a result, two populations of measurements are de facto created: an 'HRS' population corresponding to read-outs following the positive (negative) polarity programming pulses and an 'LRS' population corresponding to the opposite polarity. The devices were robust and could maintain a satisfactory window between HRS and LRS. Two different kinds of flaws were identified. In some cases a write pulse failed to alter the resistive state and in other cases both HRS and LRS drifted towards higher resistance. To address these problems and assess the endurance of these devices in an automated and less user-invasive fashion, we used a MATLAB algorithm. Endurance performance was quantified using the following method: the user defines a minimum allowed HRS-LRS opening ΔRS_{min} (in Ω) and then a MATLAB algorithm runs on the data output of the endurance routine. The algorithm systematically searches for the longest streak of continuous programming pulses for which the difference $HRS_{min} - LRS_{max} \geq \Delta RS_{min}$. An example is shown in Figure 6. The cycling endurance results from 5 devices from each device stack were evaluated for the resistance windows: 1 kOhm, 3 kOhm, 10 kOhm and 30 kOhm and are depicted in Figure 7. Each data point in Figure 7 corresponds to the cycling endurance of a device for the given resistance window. The evaluation of the devices' cycling endurance was so strict that failing to alter the resistance once led to termination of the algorithm. The results in Figure 7 reflect this strict nature of the method and possibly do not highlight the full potential of these devices but they rather provide a very conservative evaluation of the cycling endurance. However, a trend can be observed from the data. All devices with Al_2O_{3-y} layers were as good as the TiO_{2-x}-based or better. Devices with 2 Al_2O_{3-y} layers in particular, were better in cycling endurance compared to their counterparts with 1 and 3 Al_2O_{3-y} layers.

IV. DISCUSSION

During DC testing, T0 devices (TiO_{2-x}-based) showed a negative EF voltage of approximately -5.0 V (Figure 3 (a)), starting from a very insulating resistance in the range of GΩ. EF was achieved by a single negative polarity voltage sweep. T1, T2 and T3 devices comprised (Figure 3 (b)), probably due to the very strong insulating nature of Al_2O_{3-y}. The EF was carried out as a single transition and not as a 2-step or a 3-step transition, regardless of the number of Al_2O_{3-y} layers the device comprised, is an indication that the Al_2O_{3-y} layers didn't act as barriers but as a source of ionic species. Subsequently, the devices operated by toggling their internal resistance with SET and RESET operations at positive and negative polarity, respectively. SET was abrupt and required a compliance current at 100 μA to prevent an irreversible hard breakdown of the device.

The abrupt nature of SET is indicative of an abrupt physical change occurring within the active layer, that could be explained with the formation of a conductive filament (CF) [17] in the active layer. This hypothesis is also corroborated by the presence of the EF step in similar systems reported before [18, 19]. As discussed previously, from the exponential dependence of the I-V we can conclude that the filament does not have metallic properties but it can have semiconducting properties. Semiconducting filaments have also been reported previously in different oxide-based ReRAM devices [20]. Another possibility is that there is a remaining oxide gap between the CF and the electrode. The carrier conduction through this gap possibly explains the non-linear dependence of the I-V curves. This argument has been previously reported for TiO_2 systems [21]. The RESET operation is likely driven by thermal effects gradually disrupting the CFs, as also reported in similar oxide systems [20, 22]. Hence, the most feasible mechanism involves the drift of ions (oxygen vacancies) injected during the EF, creating a conductive path within the active layer.

The addition of the thin Al_2O_{3-y} layer in the device's active layer could be possibly adding Al cations in the ionic species facilitating the switching. The dissociation energy (D°_{298}) of the Al-O bonds is 501.9$\pm$10.6 $kJmol^{-1}$ compared to 666.5$\pm$5.6 $kJmol^{-1}$ of the Ti-O bonds [23], fact that could support the argument about the mobile Al cations. Moreover, it was previously suggested that the presence of Al_2O_{3-y} in a TiO_{2-x} matrix enhances the formation of oxygen vacancies resulting in lower switching voltages [2].

The EF in pulsed characterization follows a different pattern, as shown by Figure 4 (a). The triplet of pulsed voltage ramps is essential to achieve a complete EF for all device stack configurations. Following EF, the devices were able to perform a stable analog resistive switching. The presence of the EF still appears to be consistent with the observations during the DC electrical characterization. Therefore, the filamentary hypothesis for the resistive switching appears corroborated. The gradual modification of the resistance could be associated with the tuning of the oxide gap between the filament and the electrode, as we previously reported for a similar system [2].

The difference in EF between DC and pulsed operation could be sought in the different contributions of the electric field and Joule heating. During a DC voltage sweep, the voltage never drops to 0 between each step but continuously increases. The sweep is effectively a voltage staircase in which each step lasts for 1 ms. During pulsed operation, a non-invasive read pulse scheme is implemented to access the device's resistance. The read-

Figure 7. Cycling endurance results from 5 devices from each device configuration T0-T3, tested for resistance windows (a) 1 $k\Omega$, (b) 3 $k\Omega$, (c) 10 $k\Omega$ and (d) 30 $k\Omega$.

ing scheme comprises 5 read pulses with a total pulse duration and inter-pulse delay, adding up to $\sim$ 30 ms between write pulses. The estimated total energy delivered to the device due to Joule heating is in the order of 10^{-5} J, taking into account a resistive state of 200 $k\Omega$ at -5 V with 1 ms step. Additionally, the energy calculated is likely to be underestimated since just voltages in the vicinity of the threshold voltage are considered. The same approach applied to pulsed operation leads to a value in the order of 10^{-10} J. The larger inter-pulse time during pulsed operation could favour the dissipation of this energy. On the contrary, a continuous staircase would favour the heat build-up in the system.

The difference in the available energy could result in different contributions from the electric field and heat. In the case of DC operation, the generated heat rapidly induces a soft-breakdown in the oxide, without the requirement for multiple steps. Also, the heat role is corroborated by the presence of a compliance current that limits the current flow in the device, therefore preventing a hard breakdown. The 30 ms delay, allow the heat to be dissipated, pointing to an electric field-driven EF. In addition, TiO_2-based systems have been reported previously as capable of electric field-based EF [24]. The multi-step nature of EF shown in Figure 4 (a) could be ascribed to the formation of multiple filaments within the oxide film. A similar mechanism has been suggested to explain the multiple steps achieved during switching of other oxide systems [25].

In conclusion, the device operation is regulated by the formation of a conductive path within the oxide layer, which is boosted by the presence of the $Al_2O_{3\text{-}y}$ layer. $Al_2O_{3\text{-}y}$ can increase the ion/oxygen vacancy concentration available in the active layer creating a conductive path achieved by inter-diffusion during the EF. Relevant differences in the EF operations are reported, involving different driving mechanisms. During pulsed operation, EF could be achieved due to electric field-driven phenomena with little effects due to Joule heating. However, during DC operation filament formation could me more affected by Joule heating.

V. CONCLUSION

In this paper we have demonstrated that incorporation of ultra-thin $Al_2O_{3\text{-}y}$ buffer layers in $TiO_{2\text{-}x}$ active layers reduced switching voltages. The $Al_2O_{3\text{-}y}$ layers acted in a rather homogeneous way and not as solid barriers inside the active layer. The switching voltages of the devices comprising $Al_2O_{3\text{-}y}$ layers were +2.0/-2.0 V and +1.5/-1.5 V, tested with DC voltage sweeping and pulse sweeping, respectively. The $Al_2O_{3\text{-}y}$ layers were suggested to have a double role, both injecting excess oxygen vacancies but also enhancing a more repeatable and stable filament formation/eruption. Preliminary cycling endurance results suggested that $Al_2O_{3\text{-}y}$ layers possibly enhanced the devices' endurance but more work on this matter has to be carried out to reveal the full potential of these devices in endurance. The non-volatile, analog mode of switching of the devices is not limiting the devices' potential but can make them good candidates for a variety of applications in neuromorphic computing.

ACKNOWLEDGMENTS

The financial support of the EPSRC EP/K017829/1 and EU-FP7 RAMP is gratefully acknowledged.

[1] D. Acharyya, A. Hazra, and P. Bhattacharyya, Microelectronics Reliability **54**, 541 (2014).

[2] M. Trapatseli, A. Khiat, S. Cortese, A. Serb, D. Carta, and T. Prodromakis, Journal of Applied Physics **120**, 025108 (2016).

[3] I. Gupta, A. Serb, A. Khiat, R. Zeitler, S. Vassanelli, and J. . N. V. . . P. . . D. . n. Prodromakis, Themistoklis Title = Real-time encoding and compression of neuronal spikes by metal-oxide memristors, .

[4] L. Zhao, S.-G. Park, B. Magyari-Kope, and Y. Nishi, Applied Physics Letters **102**, 83506 (2013).

[5] L. Zhao, S. W. Ryu, A. Hazeghi, D. Duncan, B. Magyari-Kpe, and Y. Nishi, in *VLSI Technology (VLSIT), 2013 Symposium on* (2013) pp. T106–T107.

[6] L. Goux, A. Fantini, G. Kar, Y. Y. Chen, N. Jossart, R. Degraeve, S. Clima, B. Govoreanu, G. Lorenzo, G. Pourtois, D. J. Wouters, J. A. Kittl, L. Altimime, and M. Jurczak, in *VLSI Technology (VLSIT), 2012 Symposium on* (2012) pp. 159–160.

[7] S. Chakrabarti, D. Jana, M. Dutta, S. Maikap, Y. Y. Chen, and J. R. Yang, in *2014 IEEE 6th International Memory Workshop (IMW)* (2014) pp. 1–4.

[8] Y.-S. Chen, P.-S. Chen, H.-Y. Lee, T.-Y. Wu, K.-H. Tsai, F. Chen, and M.-J. Tsai, Solid-State Electronics **94**, 1 (2014).

[9] L.-G. Wang, X. Qian, Y.-Q. Cao, Z.-Y. Cao, G.-Y. Fang, A.-D. Li, and D. Wu, Nanoscale Research Letters **10**, 135 (2015).

[10] H. Wu, X. Li, M. Wu, F. Huang, Z. Yu, and H. Qian, IEEE Electron Device Letters **35**, 39 (2014).

[11] R. Berdan, A. Serb, A. Khiat, A. Regoutz, C. Papavassiliou, and T. Prodromakis, IEEE Transactions on Electron

482 Devices **62**, 2190 (2015).
483 [12] I. Gupta, A. Serb, R. Berdan, A. Khiat, A. Regoutz,
484 and T. Prodromakis, IEEE Transactions on Circuits and
485 Systems II: Express Briefs **62**, 676 (2015).
486 [13] A. Serb, A. Khiat, and T. Prodromakis, Electron De-
487 vices, IEEE Transactions on **62**, 3685 (2015).
488 [14] D.-H. Kwon, K. M. Kim, J. H. Jang, J. M. Jeon, M. Lee,
489 G. H. Kim, X.-S. Li, G.-S. Park, B. Lee, S. Han, M. Kim,
490 and C. S. Hwang, Nature Nanotechnology **5**, 148 (2010).
491 [15] D. Carta, G. Mountjoy, A. Regoutz, A. Khiat, A. Serb,
492 and T. Prodromakis, The Journal of Physical Chemistry
493 C **119**, 4362 (2015).
494 [16] M. Trapatseli, D. Carta, A. Regoutz, A. Khiat, A. Serb,
495 I. Gupta, and T. Prodromakis, The Journal of Physical
496 Chemistry C **119**, 11958 (2015).
497 [17] K. M. Kim, D. S. Jeong, and C. S. Hwang, Nanotech-
498 nology **22**, 254002 (2011).
499 [18] K. M. Kim, T. H. Park, and C. S. Hwang, Scientific
500 Reports **5**, 2237 (2015).
501 [19] J. J. Yang, F. Miao, M. D. Pickett, D. A. A. Ohlberg,
502 D. R. Stewart, C. N. Lau, and R. S. Williams, Nanoscale
503 Research Letters **20**, 215201 (2009).
504 [20] D. Ielmini, R. Bruchhaus, and R. Waser, Phase Transi-
505 tions **84**, 570 (2011).
506 [21] L. Qingjiang, I. Salaoru, C. Papavassiliou, X. Hui, and
507 T. Prodromakis, Scientific Reports **4**, 6 (2014).
508 [22] K. Szot, M. Rogala, W. Speier, Z. Klusek, A. Besmehn,
509 and R. Waser, Nanotechnology **22**, 254001 (2011).
510 [23] Y.-R. Luo, *Comprehensive Handbook of Chemical Bond*
511 *Energies* (Taylor and francis Group, 2007).
512 [24] S. Cortese, M. Trapatseli, A. Khiat, and T. Prodro-
513 makis, Journal of Applied Physics **120**, 065104 (2016),
514 http://dx.doi.org/10.1063/1.4960690.
515 [25] Q. Liu, C. Dou, Y. Wang, S. Long, W. Wang, M. Liu,
516 M. Zhang, and J. Chen, Applied Physics Letters **95**,
517 023501 (2009), http://dx.doi.org/10.1063/1.3176977.